Available online at www.sciencedirect.com
SCIENCE DIRECT®
Journal of Power Sources 115 (2003) 19–26
JOURNAL OF POWER SOURCES
www.elsevier.com/locate/jpowsour

Non-hydrolytic sol–gel synthesis and electrochemical characterization of tin-based oxide aerogels

John H. Harreld[a,*], Jeff Sakamoto[b], Bruce Dunn[c]

[a]Department of Chemistry, University of California, Santa Barbara, CA 93106-9510, USA
[b]Jet Propulsion Laboratory, Mail Stop 277/207, 4800 Oak Grove Drive, Pasadena, CA 91109-8099, USA
[c]Department of Materials Science and Engineering, University of California, Los Angeles, CA 90095-1595, USA

Received 14 November 2002; accepted 21 November 2002

Abstract

A non-hydrolytic sol–gel approach was utilized to create tin oxide and tin–aluminum binary oxide aerogels with high porosity (90%) and high surface area (300 m^2/g). XRD data from single-phase tin oxide aerogel indicates the growth of SnO_2 crystallites between 150 and 400 °C in air, accompanied by a substantial reduction in surface area. Heated tin oxide aerogel exhibits comparable reversible specific capacity (390 mAh/g) comparable to that of a commercially obtained SnO_2 reference (420 mAh/g). By mixing tin and aluminum precursors, binary oxide aerogels were created in which the crystal growth of tin oxide domains was suppressed until higher temperatures. The tin oxide phase in this mixed system remains electrochemically active towards lithium insertion and exhibits excellent reversibility during cycling.

1. Introduction

The development of anode materials for lithium batteries has been driven primarily by cost, safety, and energy density requirements [1–6]. In 1990, Sony Corp. developed and commercialized graphite anodes with good specific capacity and exceptional cycling stability [7]. The structure of graphite allows lithium storage between its hexagonal sheets up to a stoichiometry of LiC_6, corresponding to a specific capacity of 372 mAh/g. However, due to the formation of passivation layers during initial charging, carbons used in commercially manufactured lithium cells exhibit substantially lower reversible capacities than the theoretical amount [3].

Tin oxide systems offer higher reversible specific capacities than carbon, and the higher potential versus Li that is achieved contributes a greater margin of safety against the formation of lithium metal dendrites. The initial steps in the electrochemical reaction of lithium with tin(IV) oxide and tin(II) oxide (Equations 1 and 2, respectively) result in the formation of Li_2O [8–10]. Continued reaction with lithium results in the alloying and dealloying of lithium into tin metal (3). It is important to notice that only step (3) is electrochemically reversible.

$$4.0Li + SnO_2 \rightarrow Sn + 2Li_2O \quad (1)$$

$$2.0Li + SnO \rightarrow Sn + Li_2O \quad (2)$$

$$4.4Li + Sn \rightleftarrows SnLi_{4.4} \quad (3)$$

A great interest in tin-based composite oxides (TCO) was initiated by Fuji film's introduction of an anode material composed of Sn_2BPO_6 [11]. Later studies revealed that the active material is made up of nanoscale domains of electrochemically reduced tin metal situated in an inactive matrix of B_2O_3, P_2O_5 and Li_2O [9]. The design of active–inactive composite materials also remains a principal approach to accommodate density changes of lithium–metal systems during electrochemical cycling. In addition to tin oxide-based materials [8,12–14], prominent members of this class of anodes include Sn_2Fe:$SnFe_3C$ mixtures [15] and alloys of AB where A is a metal that alloys electrochemically with lithium and B is inert to lithium [3,16–20].

The strategy described in the present paper is to create high surface area, mixed oxides containing Sn^{2+} or Sn^{4+} centers as the active component and aluminum oxide serving as a thermally, mechanically, and electrochemically stable binder. Sol–gel chemistry provides molecular-level mixing of network precursors in addition to high surface area, high

* Corresponding author. Tel.: +1-805-893-7759; fax: +1-805-893-4120.
E-mail address: jharreld@chem.ucsb.edu (J.H. Harreld).

0378-7753/03/$ – see front matter
doi:10.1016/S0378-7753(02)00626-2

porosity microstructures. Combining tin and aluminum oxides in this way is designed to produce a fine dispersion of tin-based domains isolated from one another in a high surface area aerogel structure. The isolation of tin-based domains is intended to inhibit crystallite growth and structural coarsening at elevated temperatures, while the alumina matrix provides a compliant medium for accommodating the volume change associated with Li_2O formation.

Several traditional sol–gel approaches have been reported to produce monolithic gels [21–23] and films [24–27] of tin(IV) oxide; however, non-hydrolytic sol–gel (NHSG) chemistries are especially well suited to the synthesis of homogeneous binary oxides. The NHSG approach has been used to obtain gels of silica [28], zinc oxide [29], zirconia [30], alumina [31,32], binary oxides [33–36], and various other transition metal oxides [37]. The general approach is based on the reaction between a (semi-) metal halide and an oxygen donating species. Oxygen donors are typically dialkylethers or metal alkoxides. The polymerization reaction (Equation 4) involves the coordination and nucleophilic substitution reactions that result in the generation of bridging oxygen bonds [33,34,36,38,39]. If the metal centers are from different atoms, rapid ligand exchange reactions occur between the halides and alkoxides to form mixed alkoxyhalides (Equation 5) [40,41]. Therefore, the homogeneity of the resulting oxide is not dependent on the difference in hydrolysis rates of the precursors.

$$X_{m-1}-M-X + RO-M'-(OR)_{n-1} \rightarrow X_{m-1}-M-O-M'-(OR)_{n-1} + XR \quad (4)$$

$$M-X_m + M'-(OR)_n \rightarrow X_{m-x}-M-(OR)_x + X_x-M'-(OR)_{n-x} \quad (5)$$

In this paper we report on the application of NHSG chemistry to the synthesis of high area tin oxide and tin–aluminum binary oxides. The materials were prepared as high surface area aerogels in order to take advantage of the electrolyte accessibility and enhanced capacity observed with this morphology [42]. The tin oxide phase in the mixed system exhibits excellent lithium reversibility and offers a promising direction for the design of lithium battery anodes.

2. Experimental

Monolithic oxide gels were synthesized by non-hydrolytic condensation reactions between chlorides and alkoxides of tin or combinations of tin and aluminum. Solutions of metal chloride and metal alkoxide in *n*-methyl-2-pyrrolidinone (NMP) were prepared in an argon-filled glovebox and sealed into glass vials with poly(tetrafluoroethylene) (PTFE)-lined caps. Precursor concentrations were varied between 0.67 and 2.0 M, and in most cases the initial concentrations of halide and alkoxide groups were equivalent. The metal chlorides used were tin(II) chloride, tin(IV) chloride, tin(IV) dichlorobis(acetylacetonate), and aluminum chloride. Alkoxides used were tin(II) ethoxide, tin(IV) isobutoxide, and aluminum secbutoxide. The precursor solutions were heated to 150 °C in sealed vials. Gelled samples were aged at the same temperature for at least 24 h. Aged gels were washed thoroughly by immersion in acetone to remove unreacted precursors and alkylchloride reaction products. Aerogels were then obtained by drying washed gels from CO_2 under supercritical conditions [43].

The fraction of porosity in aerogel samples was obtained by comparing the skeletal density determined by He pycnometry (Micromeritics Accupyc 1330) with the bulk density determined by Hg pycnometry. Surface area and pore size measurements were carried out using N_2 adsorption (Micromeritics ASAP 2010) on vacuum dried specimens and analyzed by the BET method. TGA measurements (TA Instruments TGA 295) were performed in N_2 and air using a heating rate of 10 °C/min. X-ray diffraction of Cu Kα radiation (Siemens D500 diffractometer) was used to determine the oxide phases present and the degree of crystallite growth in heated samples. The size of SnO_2 crystallites in synthesized samples was estimated by using the Scherrer formula with the FWHM broadening of the (1 1 0) peak relative to the same peak in a commercially obtained crystalline SnO_2 reference (Aldrich). The ratios of Sn:Al, Sn:Cl, and Sn:C in several oxide samples were obtained by chemical analysis (Galbraith Laboratories Inc.). FTIR spectra from 4800 to 400 cm^{-1} were recorded from KCl pellets with a Nicolet 510P spectrophotometer. Transmission electron microscopy was performed using a JEOL model 100CX. TEM specimens were prepared by applying a fine dispersion of sample material in acetone onto a copper grid and allowing the solvent to dry completely.

The electrochemical performance of the oxide aerogels was characterized by galvanostatic measurements. Composite electrodes were prepared with active material (84% by mass), acetylene black carbon (10%), and PTFE (6%) dispersed in isopropanol and stirred for at least 3 days. The electrode paste was applied to copper mesh and dried under vacuum at 235 °C for at least 6 h. Reference and counter electrodes were lithium foil. The electrolyte was a 1 M solution of lithium hexafluorophosphate ($LiPF_6$) in a mixed solvent of ethylene carbonate, diethyl carbonate, and dimethyl carbonate (1:1:1, EC:DEC:DMC). The active electrode was galvanostatically discharged using a computer-controlled potentiostat/galvanostat (EG&G Princeton Applied Research, model 273A) from open circuit voltage to 0.1 V versus Li and then charged to 1.0 V versus Li. A constant current of 0.1 mA/cm^2 was used.

3. Results and discussion

Non-hydrolytic network formation occurred in several of the heated precursor solutions, resulting in monolithic gels that spanned the volume of the container (Table 1). In the

Table 1
Precursor combinations and resulting products and reaction times

Halide precursor	Alkoxide precursor	Product	Gel designation	Reaction time (days)
$SnCl_2$	$Sn(OEt)_2$	Precipitation		>1
	$Sn(O^iBu)_4$	GEL	A	1
	$Al(O^sBu)_3$	GEL	D	4
$SnCl_4$	$Sn(OEt)_2$	GEL	B	1
	$Sn(O^iBu)_4$	Stable solution		>14
	$Al(O^sBu)_3$	GEL	E	1
$SnCl_2(acac)_2$	$Sn(OEt)_2$	GEL	C	1
	$Sn(O^iBu)_4$	Stable solution		>14
	$Al(O^sBu)_3$	[a]		[a]
$AlCl_3$	$Sn(OEt)_2$	GEL	F	5
	$Sn(O^iBu)_4$	Stable solution		>14
	$Al(O^sBu)_3$	GEL		3

A capital letter designation is given to some of the gels for reference.
[a] Untested combination.

sols containing only tin precursor, it was observed that gelation occurred only when Sn^{2+} and Sn^{4+} precursors were mixed (gels "A", "B" and "C"). This effect is believed to be influenced by a competition between the ability for the metal ion to take part in network formation and the steric hindrance involved in a nucleophilic substitution on the coordinated ion. Unlike cations with higher valence, Sn^{2+} is not expected to form gel-like open networks. Thus, if reactions between Sn^{2+} compounds occur, the resulting structures may remain solvated instead of forming extended networks. On the other hand, steric inhibition is dominant when the oxygen from a bulky $Sn(O^iBu)_4$ attacks a tetrahedral $SnCl_4$. The Al^{3+} compounds appear to fit well between the competing factors of bond reactivity and steric effects. Sols which contained aluminum formed intact gels in all the precursor combinations tested with the exception of $AlCl_3$ and $Sn(O^iBu)_4$, where the coordination reaction is likely to be restricted by the bulk of the alkoxide ligands.

Supercritical solvent extraction from the monolithic gelled samples resulted in amorphous aerogels with high surface area, high porosity. The structural characterization data from BET and pycnometric analyses are summarized in Table 2. This table shows the structural response of these materials to various heat treatments in air. Due to the presence of unreacted surface groups (chlorine and alkoxide), the gels exhibited between 10 and 30% mass loss up to 600 °C in air (Fig. 1). The aerogels from a sol containing only tin precursors (gels "A", "B" and "C") were nearly identical in terms of amount of TGA mass loss, pore size, and specific surface area (Table 2). XRD data diffraction data were obtained from these materials after they were heated in air to temperatures in the range of 150 to 700 °C (Fig. 2). As-dried materials (150 °C) are mostly amorphous but contain very small crystallites (less than 10 nm) of SnO_2. Further growth of the existing crystals was observed by 400 °C (Fig. 3) and continues to a size of almost 50 nm at 700 °C.

Table 2
Physical structural data obtained from non-hydrolytically derived gels using BET, He and Hg pycnometric, and TGA analyses

Gel	T (°C in air)	S (m^2/g)	Porosity (%)	Pore size (nm)	TGA mass loss at 600 °C (%)
A	150	290	92	165	15
	400	125	[a]	240	
	600	40	93	150	
B	150	310	[a]	165	16
C	150	290	[a]	150	[a]
D	150	170	95	100	30
	600	210	97	105	

[a] Not measured.

It is desirable understand the effects of processing on the tin oxidation state, which contributes to lost lithium capacity (Equations 1 and 2). FTIR spectra from these samples reveal the occurrence of a rearrangement in Sn–O bonding structure during heat treatment (Fig. 4). The SnO_2 reference (Fig. 4f) exhibits Sn–O vibrational bands centered at approximately 625 and 675 cm^{-1}. As the dried tin oxide aerogel is heated, the band at 625 cm^{-1} becomes more clearly defined but the vibration at 675 cm^{-1} was still unresolved. After heating to 600 °C, the material was not completely crystallized and a significant amount of disorder remains relative to the commercially obtained crystalline powder (Fig. 2). The vibrational spectra indicate the gradual appearance of a band edge from around 600 cm^{-1} to lower energy in tin oxide aerogels heated up to at least 400 °C Fig. 4a–d. This band edge matches that of the commercially obtained crystalline SnO powder (Fig. 4e). This suggests that the Sn–O bonding structure of the aerogel may contain some bonding characteristics of SnO as well as SnO_2. Amorphous tin oxide compositions between SnO and SnO_2 have been described in the literature [44,45]. This band is apparently lost on heating to 700 °C as would be expected from the well-known disproportionation reaction (Equation 6) [44–49]. Discrete crystalline domains of SnO have not been detected by XRD analyses of samples heated in N_2.

$$2SnO \rightarrow Sn + SnO_2 \quad (6)$$

The mixed oxide gels from a sol containing mixed precursors of tin and aluminum (gels "D", "E" and "F") exhibited a wide range of compositions and very different responses to thermal treatments. Samples from $SnCl_2$ and $Al(O^sBu)_3$ (gel "D") were transparent immediately after gelation, whereas all of the other NHSG-derived gels obtained were opaque. After these transparent gels had been left at 150 °C for 3 days, they too became opaque. The FTIR data from gel "F" (Fig. 4g) show a band structure between those of crystalline reference powders of pure SnO_2 and Al_2O_3 (Fig. 4h and i, respectively).

A series of gels from $Sn(OEt)_2$ and $AlCl_3$ (gel "F") were prepared using various precursor ratios and concentrations

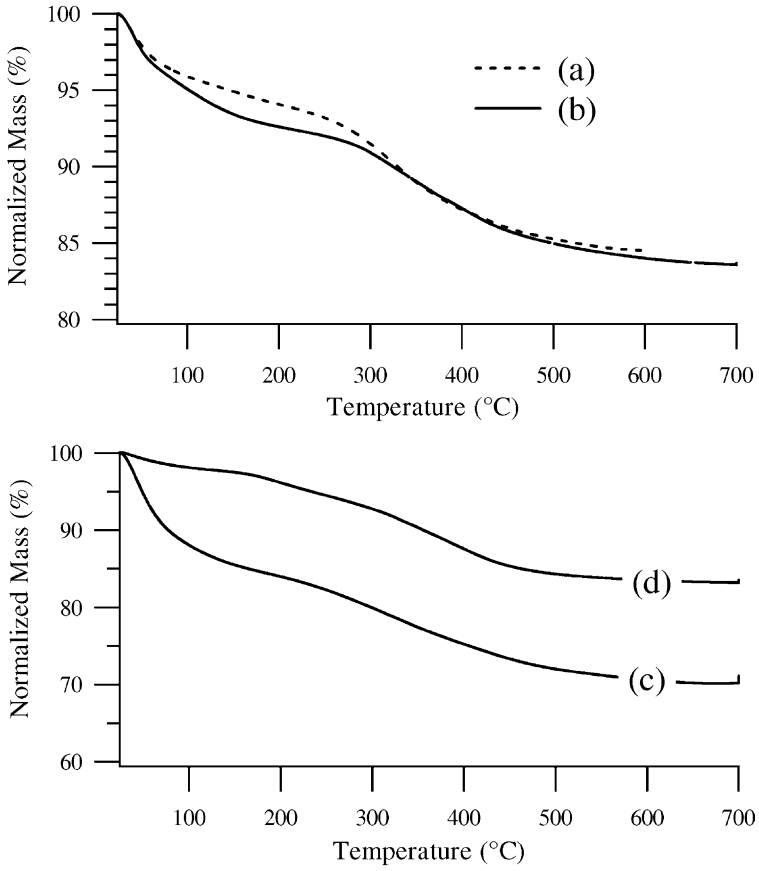

Fig. 1. TGA data for various aerogels synthesized from tin-based precursor solutions (top) or from mixtures of tin- and aluminum-based precursor (bottom). The gels are labeled according to the designations in Table 1.

in order to determine: (i) the effect of the fraction of aluminum oxide on the crystallization behavior of the tin oxide; and (ii) the synthesis parameters required to obtain material of a desired composition. The compositions of the resulting dried gels are compared to the corresponding sol compositions in Fig. 5. In all samples measured, the ratio of Sn:Al is lower in the dried gel than in the initial sol. Under these synthetic conditions, a two-fold excess of tin-based precursor is required to obtain a final target composition of $SnAlO_{3.5}$. Similar results were demonstrated by hydrolytic

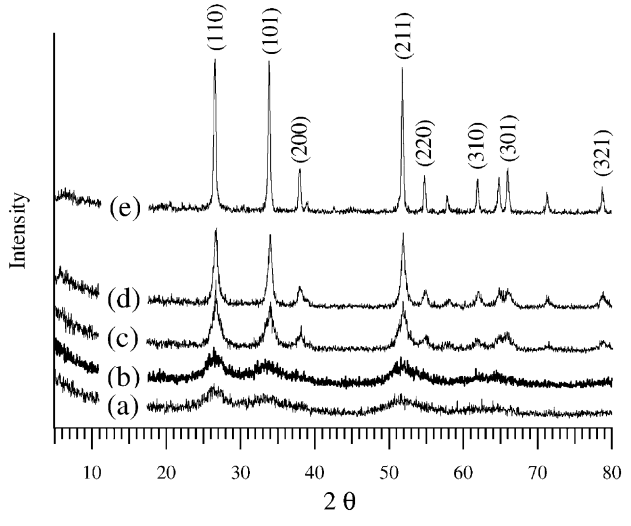

Fig. 2. XRD patterns from tin oxide aerogel (gel "A") after being heated in air to (a) 150 °C, (b) 200 °C, (c) 400 °C, and (d) 700 °C. Curve (e) is commercially obtained crystalline SnO_2.

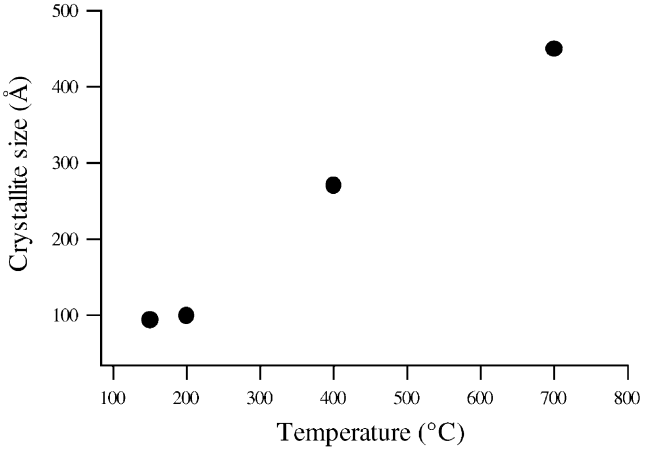

Fig. 3. Change of crystallite size for a tin oxide aerogel (gel "A" heated in air from 150 to 700 °C).

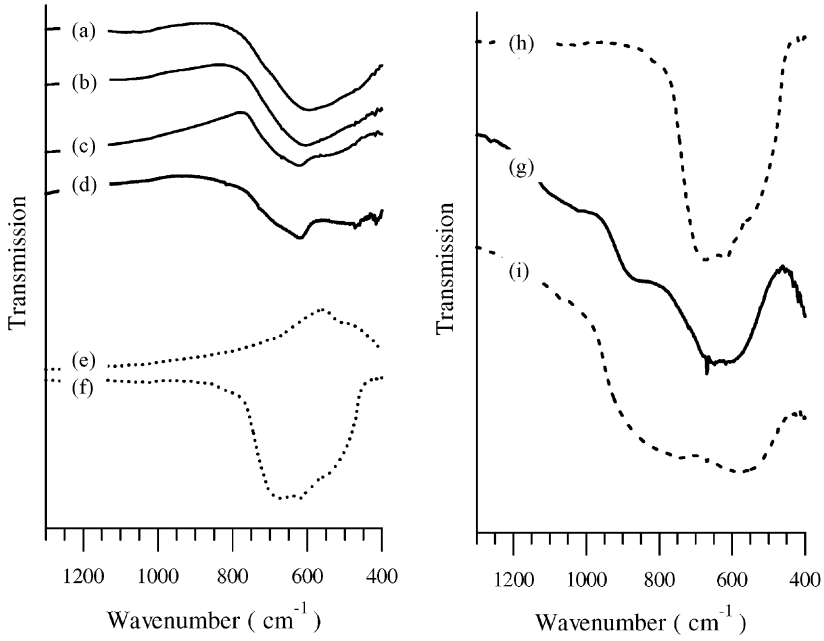

Fig. 4. FTIR spectra from tin oxide xerogel after being heated in air to (a) 150 °C, (b) 200 °C, (c) 400 °C, and (d) 700 °C; included for reference are spectra from commercially obtained crystalline powders of (e) SnO and (f) SnO_2 (left side). FTIR spectra from (g) mixed oxide xerogel "F" and commercially obtained crystalline powders of (h) SnO_2 and (i) Al_2O_3 (right side).

sol–gel syntheses of tin-doped alumina in which $SnCl_4$ was reacted with pre-hydrolyzed $Al(O^iPr)_3$ [50].

The crystallization temperature of these materials is greatly dependent on the ratio of Sn:Al in the mixed oxide. As the aluminum oxide content is increased, the crystallization of the SnO_2 phase is suppressed to higher temperatures (Fig. 6), whereas the alumina network remains amorphous. An aerogel having a composition of about 1:1 Sn:Al begins to crystallize by 400 °C (similar to data from SnO_2 aerogel, Figs. 2 and 3), while an aerogel having a composition of about 1:6 Sn:Al is amorphous up to 650 °C. The latter is consistent with NHSG-derived alumina gels reported by Acosta et al. [34] that remained amorphous up to 750 °C. Thus, the behavior of our materials can be explained by the presence of well-dispersed domains of tin oxide in the aluminum oxide phase. The loss of surface area during heating was also reduced by the presence of the aluminum oxide. The specific surface area of the tin oxide aerogel was reduced from 290 to 40 m^2/g after being heated to 600 °C, whereas the mixed oxides all exhibited surface areas between 100 and 210 m^2/g at the same temperature. The microstructure of tin oxide and mixed oxide aerogels was examined by TEM analysis and found in each case to consist of interconnected particles that are primarily on the order of tens of nanometers (Fig. 7). The structural coarsening observed from the BET and XRD data of tin oxide samples is confirmed by comparing the TEM images of sample heated to 150 and 600 °C (Fig. 7a and b). The microstructural evolution of the mixed oxide from 150 to 600 °C (Fig. 7c and d) indicates an increase in fine structure (however, note the scale change) and is attributed to the growth of nanometer-scale SnO_2 crystallites.

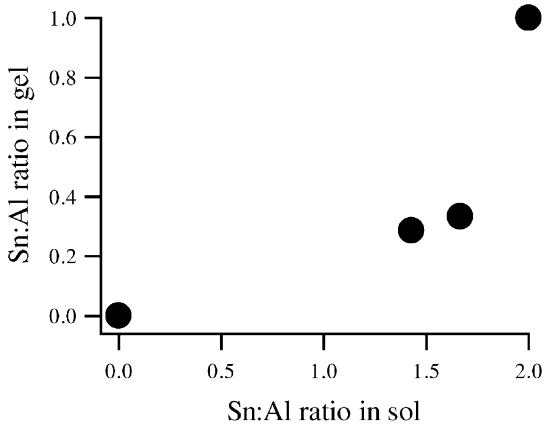

Fig. 5. Comparison of the Al:Sn ratio in washed gels (obtained by chemical analysis data) and that of the corresponding initial solutions. The data indicate a significant preference for Al^{3+} inclusion in the gel network.

One of the tin oxide aerogels (gel "A") was prepared as an electrode for galvanostatic testing and compared to an electrode that incorporated commercial SnO_2 powder. The tin oxide aerogel and the SnO_2 reference material exhibit a similar potential response during the initial discharge and first charge step (Fig. 8). The reversible specific capacity of the aerogel was comparable to that of the commercial powder measured in the same potential window (Table 3). In both the aerogel and the powder samples, a high irreversible capacity and a large degree of swelling of the working electrode were observed during the initial discharge. Both effects are attributed to the formation of Li_2O.

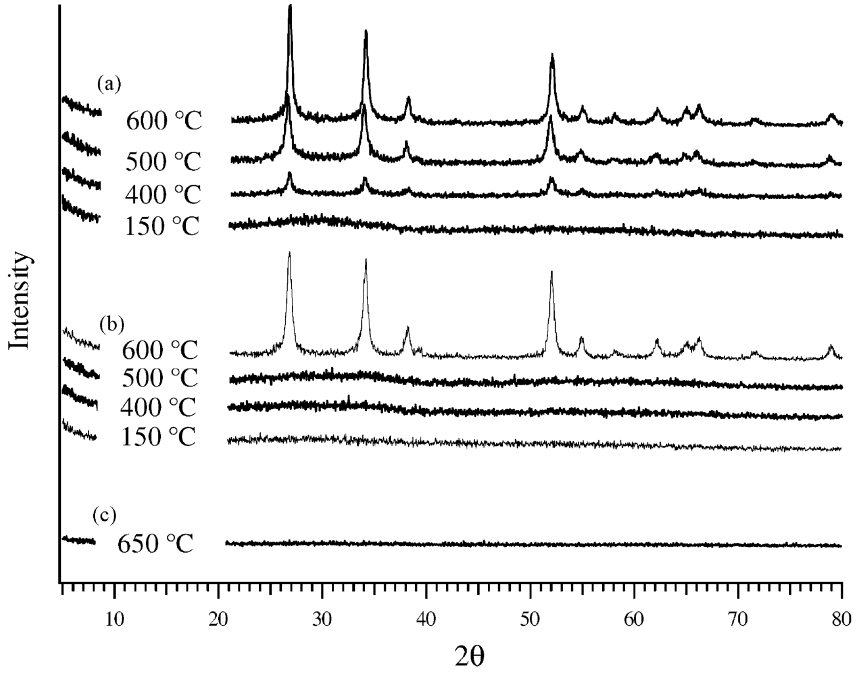

Fig. 6. XRD patterns showing the different ranges of crystallization temperature for tin–aluminum mixed oxide aerogels with the following Sn:Al ratios: (a) 1:1, (b) 1:3 and (c) 1:6.

Galvanostatic discharge experiments were carried out using two of the binary oxide aerogels (gels "D" and "F") The Sn:Al ratio of both gels were approximately 1:3. Both compositions were active towards lithium insertion and exhibited excellent reversibility on cycling. The data from gel "D" is presented in Fig. 8b. Table 3 compares the initial and reversible specific capacities of the tin–aluminum mixed oxides with the tin oxide aerogel and the SnO_2 reference material.

It is evident from Table 3 that the lithium activities for the mixed oxide aerogels are substantially lower than that of the corresponding tin oxide aerogel. At a Sn:Al ratio the mass

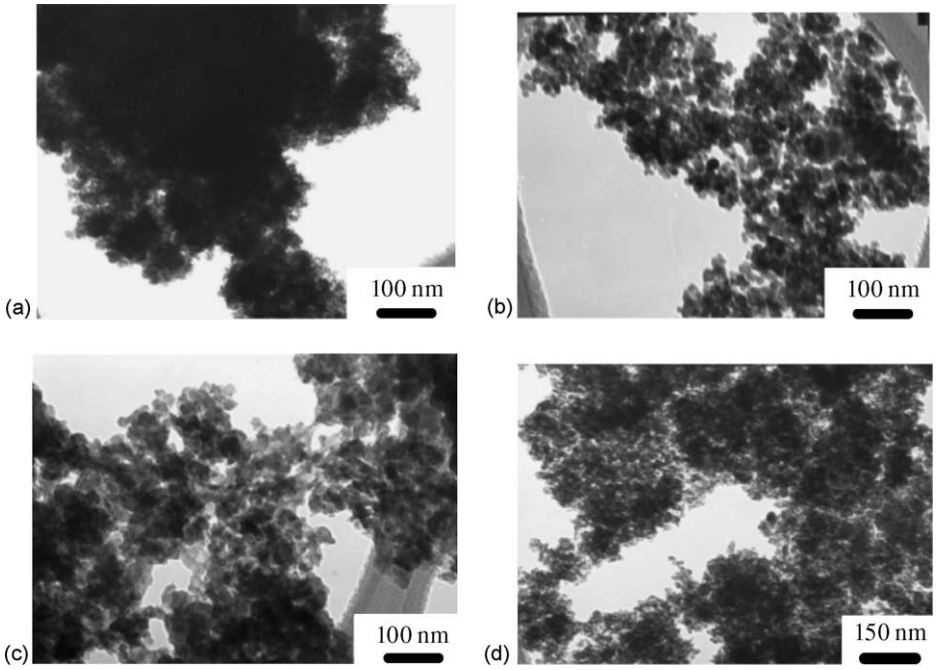

Fig. 7. TEM images of tin oxide aerogel "C" after heating to (a) 150 °C and (b) 600 °C, and of mixed oxide aerogel "D" after heating to (c) 150 °C and (d) 600 °C.

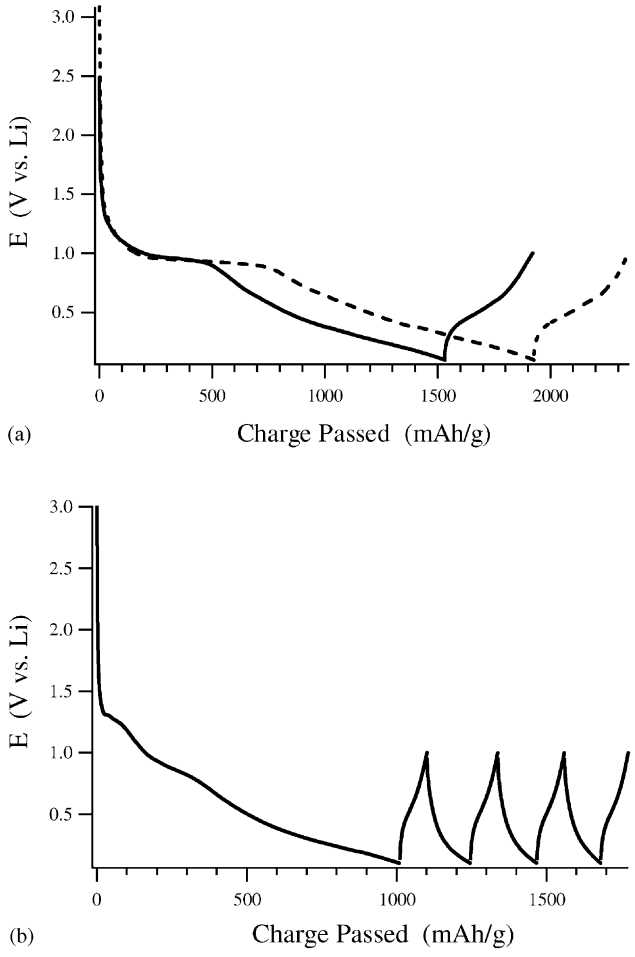

Fig. 8. Galvanostatic cycling data for tin oxide and binary tin–aluminum oxide aerogel. (a) Comparison of initial discharge and first charge for tin oxide aerogel (solid line) and crystalline SnO_2 reference (dashed line). (b) Initial discharge and four charge–discharge cycles for tin–aluminum mixed oxide aerogel "D".

fraction of SnO_2 is approximately 50% and the best mixed oxide composition (F) has ~30% of the specific capacity of the tin oxide aerogel. This suggests that a significant fraction of the dispersed tin oxide domains are isolated and not electrochemically accessible, especially since prior work with V_2O_5 aerogel electrodes showed that the mesoporous morphology of the aerogel facilitates electrolyte penetration through the aerogel electrode [51]. Thus, it is likely that the low capacities of the mixed oxide aerogels arise from the inability to provide a continuous electronic path to the dispersed tin oxide phase. One means of rectifying this situation is to prepare materials with a higher fraction of the conductive tin oxide phase. Another approach is to add a greater amount of carbon black to the electrode in order to provide a better electronic conducting network. The use of carbon nanotubes should also be effective for this purpose and are less likely to occlude the tin oxide domains [51].

Table 3
Initial and reversible specific capacity for electrochemically cycled tin oxide aerogel materials

Composition (sample)	Specific capacity (mAh/g)		
	Initial	Reversible (by total mass)	Reversible (by SnO_2 mass)
SnO_2 (crystalline reference)	1900	420	420
SnO_2 (gel A)	1500	390	390
SnO_2*1.5Al_2O_3 (gel D)	980	91	180
SnO_2*1.5Al_2O_3 (gel F)	1400	130	240

Initial capacity is based on initial discharge from open circuit voltage to 0.1 V versus Li, and reversible capacities are based on cycling within the potential range of 0.1–1.0 V vs. Li.

4. Conclusions

A characteristic of non-hydrolytic sol–gel chemistry is that two metal centers, each with different reactivity, can be combined into homogeneous gels. By mixing precursors with tin and aluminum centers, mixed oxides can be created which exhibit the beneficial properties of either phase. The amorphous state of tin oxide aerogel is stabilized to higher temperatures when aluminum oxide is incorporated into the structure (1:3 Sn:Al increases the crystallization temperature to 500–600 °C). The tin oxide phase remains electrochemically active towards lithium insertion and exhibits excellent reversibility during cycling.

The current work provides design rules for multi-phase materials in which the electrochemically active (tin oxide) is dispersed within an electrically insulting phase (the alumina aerogel matrix). There must be sufficient tin oxide present to achieve electronic accessibility to all of the active phase so that that a high specific capacity is obtained. Moreover, to ensure adequate electronic conduction throughout the electrode, the addition of greater amounts of carbon black or perhaps carbon nanotubes will be helpful. The aluminum oxide phase must be present in a sufficient amount to suppress crystallization of the tin oxide during heating and to provide a porous matrix for volumetric stability during cycling. Future development will involve defining the optimal composition of the mixed oxide between 1:0.7 and 1:3 Sn:Al. An intriguing possibility is that the porous morphology of these materials enables the use of liquid- or gas-phase reduction treatments to transform the tin from 4^+ to either 2^+ or the metallic state. The resulting structure is likely to be a finely distributed nanoscale dispersion of a highly active tin phase in a stable, high surface area binder of alumina.

Acknowledgements

The authors would like to thank the Office of Naval Research for the financial support of this work. Dr. Wei Cheng deserves special thanks for contributing her expertise in TEM analysis.

References

[1] B. Scrosati, J. Electrochem. Soc. 139 (1992) 2776.
[2] K. Brandt, Solid State Ionics 69 (1994) 173.
[3] S. Megahed, S.P. Armes, J. Power Sources 51 (1994) 79.
[4] M. Winter, J.O. Besenhard, Electrochem. Acta 45 (1999) 31.
[5] B.B. Owens, W.H. Smyrl, J.J. Xu, J. Power Sources 81–82 (1999) 150.
[6] J.-M. Tarascon, M. Armand, Nature 414 (2001) 359.
[7] T. Nagaura, K. Tozawa, Prog. Batteries Solar Cells 9 (1990) 209.
[8] I.A. Courtney, J.R. Dahn, J. Electrochem. Soc. 144 (1997) 2045.
[9] I.A. Courtney, J.R. Dahn, J. Electrochem. Soc. 144 (1997) 2943.
[10] J. Wolfenstine, J. Sakamoto, C.-K. Huang, J. Power Sources 75 (1998) 181.
[11] Y. Idota, T. Kubota, A. Matsufuji, Y. Maekawa, T. Miyasaka, Science 276 (1997) 1395.
[12] S.D. Han, S.Y. Huang, G. Campet, S.H. Pulcinnelli, C.V. Santilli, Active Passive Elec. Comp. 18 (1995) 61.
[13] J.S. Sakamoto, C.K. Huang, S. Surampudi, M. Smart, J. Wolfenstine, Mater. Lett. 33 (1998) 327.
[14] N. Li, C.R. Martin, B. Scrosati, J. Power Sources 97–98 (2001) 240.
[15] O. Mao, R.L. Turner, I.A. Courtney, B.D. Fredericksen, M.I. Buckett, L.J. Krause, J.R. Dahn, Electrochem. Solid State Lett. 2 (1999) 3.
[16] A.N. Dey, J. Electrochem. Soc. 118 (1971) 1547.
[17] G.X. Wang, L. Sun, D.H. Bradhurst, S. Zhong, S.X. Dou, H.K. Liu, J. Power Sources 88 (2000) 278.
[18] J. Wolfenstine, S. Campos, D. Foster, J. Read, W.K. Behl, J. Power Sources 109 (2002) 230.
[19] D.G. Kim, H. Kim, H.-J. Sohn, T. Kang, J. Power Sources 104 (2002) 221.
[20] N. Tamura, R. Ohshita, M. Fujimoto, S. Fujitani, M. Kamino, I. Yonezu, J. Power Sources 107 (2002) 48.
[21] J.G. Giuntini, W. Ganier, J.V. Zanchetta, A. Taha, J. Mater. Sci. Lett. 9 (1990) 1383.
[22] Y. Kobayashi, M. Okamoto, A. Tomita, J. Mater. Sci. 31 (1996) 6125.
[23] N.-L. Wu, L.-F. Wu, Y.-C. Yang, S.-J. Huang, J. Mater. Res. 11 (1996) 813.
[24] B. Orel, U. Lavrencic-Stangar, Z. Crnjak-Orel, P. Bukovec, M. Kosec, J. Non-Cryst. Solids 167 (1994) 272.
[25] T.D. Senguttuvan, Thin Solid Films 289 (1996) 22.
[26] K. Tsukuma, T. Akiyama, H. Imai, J. Non-Cryst. Solids 210 (1997) 48.
[27] T.M. Racheva, G.W. Critchlow, Thin Solid Films 292 (1997) 299.
[28] R.J.P. Corriu, D. Leclercq, P. Lefevre, P.H. Mutin, A. Vioux, J. Non-Cryst. Solids 146 (1992) 301.
[29] S.C. Goel, M.Y. Chiang, P.C. Gibbons, W.E. Buhro, Mater. Res. Soc. Symp. Proc. 271 (1992) 3.
[30] M. Janson, E. Guenther, Chem. Mater. 7 (1995) 2110.
[31] S. Rezgui, B.C. Gates, S.L. Burkett, M.E. Davis, Chem. Mater. 6 (1994) 2390.
[32] S. Acosta, P. Arnal, R.J.P. Corriu, D. Leclercq, P.H. Mutin, A. Vioux, Mater. Res. Soc. Symp. Proc. 364 (1994) 43.
[33] R.J.P. Corriu, D. Leclercq, P. Lefevre, P.H. Mutin, A. Vioux, J. Mater. Chem. 2 (1992) 673.
[34] S. Acosta, R.J.P. Corriu, D. Leclercq, P. Lefevre, P.H. Mutin, A. Vioux, J. Non-Cryst. Solids 170 (1994) 234.
[35] R.J.P. Corriu, D. Leclercq, Angew. Chem. Int. Ed. Engl. 35 (1996) 1420.
[36] R.J.P. Corriu, D. Leclercq, P. Lefevre, P.H. Mutin, A. Vioux, Chem. Mater. 4 (1992) 961.
[37] P. Arnal, R.J.P. Corriu, D. Leclercq, P.H. Mutin, A. Vioux, Mater. Res. Soc. Symp. Proc. 364 (1994) 339.
[38] P. Arnal, R.J.P. Corriu, D. Leclercq, P.H. Mutin, A. Vioux, Chem. Mater. 9 (1997) 694.
[39] J.N. Hay, H.M. Raval, J. Mater. Chem. 8 (1998) 1233.
[40] D.C. Bradly, D.A.W. Hill, J. Am. Chem. Soc. 85 (1963) 2101.
[41] H. Weingarten, J.R. Van Wazer, J. Am. Chem. Soc. 87 (1965) 724.
[42] D.R. Rolison, B. Dun, J. Mater. Chem. 11 (2001) 963.
[43] N. Husing, U. Schubert, Angew. Chem. Int. Ed. Engl. 37 (1998) 22.
[44] N.S. Chaudhury, R.P. Goehner, N. Lewis, R.W. Green, Thin Solid Films 122 (1984) 231.
[45] S. Muranaka, Y. Bando, T. Takada, Nippon Kagaku Kaishi 11 (1987) 1886.
[46] L.G. Berezkina, N.I. Ermakova, D.M. Chizhikov, Zh. Neorgan. Khim. 9 (1964) 1760.
[47] Z.P. Titova, E.V. Savina, D.N. Klushin, Zh. Prikl. Khim. 37 (1964) 2150.
[48] D. Tao, X. Yang, Zhongguo Youse Jinshu Xuebao 8 (1998) 126.
[49] C. Mallika, A.M. Edwin Shuresh Raj, K.S. Nagaraja, O.M. Sreedharan, Thermochim. Acta 371 (2001) 95.
[50] M. Haneda, S. Ohzu, Y. Kintaichi, K. Shimizu, J. Shibata, H. Yoshida, H. Hamada, Bull. Chem. Soc. Jpn. 74 (2001) 2075.
[51] J.S. Sakamoto, B. Dunn, J. Electrochem. Soc. 149 (2002) A26.